

不同自由度琼斯矩阵超构表面结构设计及应用

包燕军*, 李宝军**

暨南大学纳米光子学研究院广东省纳米光学操控重点实验室, 广东 广州 511443

摘要 超构表面是人工设计的二维平面结构, 可为光学器件的小型化和集成化提供新的思路。近年来, 随着这一领域的不断发展, 基于超构表面光学的各种光场调控机理和功能器件被提出。本文以光场操控的琼斯矩阵自由度为出发点, 对近十年来的超构表面光学进展进行归类和综述, 总结不同自由度琼斯矩阵的设计方法和相应的应用, 并展望多自由度的超构器件研究的发展趋势。

关键词 超构表面; 琼斯矩阵; 多自由度; 相位调控; 振幅调控

中图分类号 O436 文献标志码 A

DOI: 10.3788/AOS230845

1 引言

光集成器件在现代信息通信和计算中扮演着重要的角色, 随着人们对信息处理和计算速度的要求不断提高, 光器件的小型化和功能集成化成为必然趋势。基于自然材料的传统光学器件存在着尺寸大、效率低、功能单一等问题, 如何在亚波长尺度高效地对光场的各种属性进行灵活操控是一个重要研究课题。2011年, 哈佛大学 Capasso 课题组^[1]提出一种亚波长厚度的金属微纳结构, 实现了广义折射定律; 次年, 复旦大学周磊教授课题组^[2]提出梯度型的人工金属结构, 将自由空间的平面波转化为表面波。这些工作开创了超构表面 (metasurface) 这一研究方向。超构表面是人工设计的由具有特殊电磁属性的原子组成的二维平面结构, 能够在亚波长尺度范围内对光场的各种光学属性如振幅、偏振和相位等进行灵活调控。更为重要的是, 其独特的二维平面结构特性解决了传统的基于自然材料光学器件体积大等问题, 为光学器件的小型化和集成化提供了新的解决方案, 因此在光学领域有着良好的应用前景。

目前, 超构表面光学已发展成为一个热门研究方向, 并受到人们的广泛关注。谷歌学术检索显示, 目前已发表的与超构表面相关的文章有五万多篇。在这些研究论文中, 研究人员提出了各种各样的光场调控机理, 实现了种类繁多的光学功能及应用^[3-20], 同时也有众多的综述从不同角度对这些研究进行了总结^[21-30]。这些光场调控看似功能迥异、各有不同, 但在数学上都

可以用一个 2×2 的琼斯矩阵统一描述^[31], 而这些不同的功能都可归纳于不同自由度琼斯矩阵的调控。琼斯矩阵通常用于描述光学器件对光的偏振、振幅、相位的调控能力 [图 1(a)], 共包含 8 个参数自由度。能调控的自由度越多, 意味着对光场的调控能力越强, 所能实现的功能也越丰富 [图 1(b)]。例如, 基于琼斯矩阵的 x, y 分量的相位调控可以实现 y 偏振入射、 x 偏振反常透射, 这即是 2011 年提出广义折射定律的论文中的结果^[1], 其可归属于单一的琼斯矩阵自由度。当琼斯矩阵自由度提升到两个时, 比如实现其某个分量的振幅和相位的独立调控^[32], 则可应用于彩色打印图像和全息图像的集成。显然, 实现更高自由度琼斯矩阵能带来更强大的光场调控能力和更丰富的功能。因此, 本文以对琼斯矩阵的自由度调控为出发点, 从设计和应用两个角度对目前超构表面的研究进行分类和总结, 并简要展望未来多自由度超构表面的发展趋势。

2 不同自由度琼斯矩阵超构表面的构造及应用

2.1 单自由度

琼斯矩阵包含 4 个分量, 每个分量又包含振幅和相位两个参量, 因此对于具有单个自由度的琼斯矩阵结构来说, 其只能调控某一个分量的相位或者振幅。对于相位调控, 目前主要有两种机制, 分别是几何相位 [图 2(a)] 和共振 (或传输) 相位 [图 2(b)、(c)]。几何相位描述了一个具有转角为 θ 的结构, 当入射光为左旋光或者右旋光时, 其透射的正交偏振态分量, 即右旋

收稿日期: 2023-04-19; 修回日期: 2023-05-23; 录用日期: 2023-05-29; 网络首发日期: 2023-06-23

基金项目: 国家自然科学基金 (92150107, 62075246)、广东省自然科学基金 (2022B1515020019)、广州市科技计划项目 (202201010361)

通信作者: *yanjunbao@jnu.edu.cn; **baojunli@jnu.edu.cn

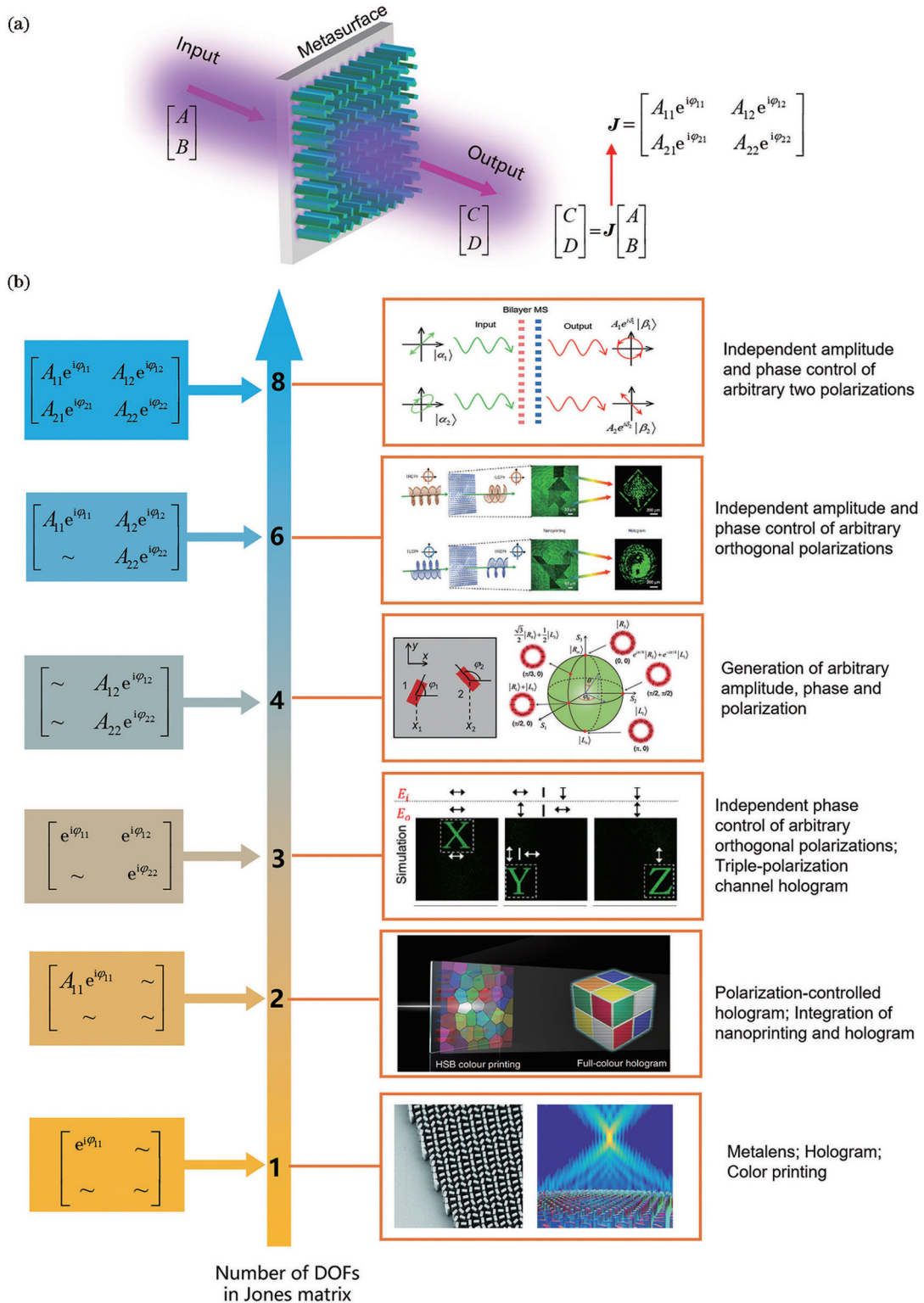


图 1 基于超构表面结构的光场调控。(a) 超构表面对光场的调控可以用一个 2×2 的琼斯矩阵描述,其建立了入射光和出射光属性(振幅、相位和偏振)之间的联系;(b) 不同自由度琼斯矩阵超构表面实现不同的光学功能

Fig. 1 Optical manipulation based on metasurface. (a) Optical manipulation by metasurface can be described by a 2×2 Jones matrix, which establishes the relationship between the properties of incident and output lights; (b) realization of different optical functionalities by metasurface with different degrees of freedom (DOFs) in Jones matrix

光或左旋光,将附加一个 $\pm 2\theta$ 的转角相位^[33],其中转角相位前面的正负号取决于入射光的圆偏振态。在以圆偏振光为基矢的情况下,其琼斯矩阵可以写成

$$\begin{bmatrix} \sim & e^{i2\theta} \\ e^{-i2\theta} & \sim \end{bmatrix}$$

其中浪纹线(\sim)表示不具备调控的自由度。

虽然该琼斯矩阵非对角项的两个分量的相位可调,但

由于相互共轭,不具备独立的调控性能,因此只能算作单个自由度。几何相位和形状无关,只要不具备高度的对称性(如正方形、圆形),都具有覆盖完整的 2π 相位的调控能力,其中最常见的是图 2(a) 所示的纳米棒结构。几何相位的这一随转角相位可调的简易特性使其在光场调控领域得到广泛的应用。在超透镜成像应用方面^[34-41],2016 年哈佛大学的 Capasso 课题组^[35]基于二氧化钛纳米棒的几何相位超构表面实现了在整个光频都接近衍射极限的透镜聚焦功能,数值孔径达到 0.8,效率达到 86%,成像质量可媲美当前主流的商业透镜[图 2(d)]。在全息成像领域^[42-51],基于反射式的几何相位,超构表面可将全息效率提升到 80% [图 2(e)]^[45],这一效率突破了传统二元结构计算全息的理论上限值 40.5%,显示了超构表面结构在全息领域的颠覆性作用。对于引言中提到 V 形天线结构^[1],通过调控其开口角度和转角实现了入射 y 偏振、反常折射 x 方向偏振的光输出,其对应的单个自由度琼斯矩阵为 $\begin{bmatrix} \sim & e^{i\varphi} \\ \sim & \sim \end{bmatrix}$ 。这种方案需要精细地设计每一个单元结构的纳米结构尺寸,然而基于几何相位设计,这一功能则变得十分简单^[52-55]。通过构造转角依次递增的纳米棒结构^[52],而无需精细设计纳米棒的结构尺寸,即可实现圆偏振入射下的反常折射[图 2(f)]。由于几何相位只附加在偏振转换的分量中,因此入射左旋光时,其透射的同偏振态光仍然满足正常的折射定律,只有透射光的右旋偏振态实现了反常折射,方向在正常折射光的左侧。当入射光变为右旋偏振态后,几何相位符号翻转,因此透射的左旋光将实现反常折射,且附加相反的水平波矢,导致其折射方向在正常折射光的右侧[图 2(f)]。几何相位与波长无关,因此该反常折射现象是宽波段可观测的。除此之外,几何相位还可应用于诸多领域,实现图像边缘探测^[56-58]、涡旋光产生^[59-63]等功能。

除了几何相位,还有一种常用的相位产生机制,即共振相位或传输相位。共振相位通过改变结构的尺寸及形状,如纳米棒的长度、圆盘的半径等[图 2(b)、(c)],使其在特定单个波长下发生连续的相位改变。至于能否实现完整的 2π 相位差改变,取决于结构的尺寸范围和波长的选择是否合适。在实际设计中,需要预先计算出结构在不同尺寸下的相位改变的数据库,然后根据相位需求找到对应的结构尺寸,从而实现功能的设计。显然该方法要比基于几何相位的设计更复杂。从本质来看,上述讨论的 V 形天线结构^[1]通过调控开口角度和转角的方法也属于共振相位调控机制。

基于共振相位的光场调控也得到了广泛应用^[64-78]。如图 2(g) 所示,通过改变纳米棒的长度,实现了 2π 的相位差改变,将纳米棒按照相位等间隔排列成周期结构后,能够实现反常反射^[67]。由于采用了三明治的反射结构,其正常的零级反射得到了很好的抑制,

理论上能达到完美的接近 100% 的反常反射。但由于采用了共振相位机制,这一反常反射只能工作在很窄的波段内,无法像基于几何相位那样实现宽波段的反常现象。除了纳米棒结构,通过改变圆盘的半径^[73, 79-80]也能够保持高透射率的前提下产生不同的相位,从而生成全息图像^[73],如图 2(h) 所示。

纳米棒结构和圆盘结构除了调控光场的相位外,通过改变尺寸也能够调控其振幅[图 2(c)]。这种振幅的调控能力在不同波长下是不一样的,因此从整个可见光光谱来看,当结构尺寸改变时,不同波长下的振幅会发生不同的改变,最终导致结构色变化,这一效应被应用于纳米结构的彩色印刷显示领域^[81-90]。如图 2(i) 所示,改变纳米棒的长度,其周期结构在偏振平行纳米棒长度的入射光照射下(y 方向)会显示出不同的颜色^[82]。由于纳米棒宽度固定,当入射 x 偏振光时,其颜色几乎不发生变化,因此该结构色是偏振依赖的。对于圆盘结构,由于具有对称性,其对入射光的偏振是不敏感的。图 2(j)、(k) 为基于圆盘结构实现全彩图像显示的结构和实验效果图,其可以对一些色彩丰富的世界名画进行高度复原^[84, 90]。上述结构由于其琼斯矩阵只实现了单一自由度的调控,因此实现的功能较为单一,或者实现的不同功能之间相互关联。为了实现更多功能的集成,需要提升结构的琼斯矩阵自由度。

2.2 双自由度

以纳米棒结构为例,探讨如何构造两个自由度的琼斯矩阵。纳米棒结构具有 3 个几何自由度:转角、长轴及短轴的长度。在固定转角的情况下,通过改变长轴和短轴的长度来独立调控这两个垂直方向的传输相位 φ_1 和 φ_2 [图 3(a)],实现两个自由度的琼斯矩阵构造,其对应的琼斯矩阵为 $\begin{bmatrix} e^{i\varphi_1} & \sim \\ \sim & e^{i\varphi_2} \end{bmatrix}$ 。这一特性可被用于生成偏振调控的双全息图像^[91],如图 3(e) 所示。当入射光的偏振态为 x 偏振态时,生成“NTU”图案的全息图;当入射光偏振态切换为 y 偏振态时,全息图像变为“RCAS”。前面已提到,当改变纳米棒尺寸时,除了改变其传输相位,还可以改变其振幅,实现不同颜色变化。因此,通过调控纳米棒的长短轴长度,可以在两个正交线偏振态下独立调控振幅[图 3(b)],即结构色,实现立体图像的 3D 显示^[92][图 3(f)],相应的琼斯矩阵可表示为 $\begin{bmatrix} A_1 & \sim \\ \sim & A_2 \end{bmatrix}$ 。

当引入转角自由度 θ ,并考虑纳米棒两个方向独立的传输相位 φ_1 和 φ_2 ,此时琼斯矩阵为

$$J = R(-\theta) \begin{bmatrix} e^{i\varphi_1} & \sim \\ \sim & e^{i\varphi_2} \end{bmatrix} R(\theta), \quad (1)$$

式中: $R(\theta)$ 为旋转矩阵, $R(\theta) = \begin{bmatrix} \cos \theta & \sin \theta \\ -\sin \theta & \cos \theta \end{bmatrix}$ 。当入射光为圆偏振光 $[1, \pm i]^T$ 时,其出射光为

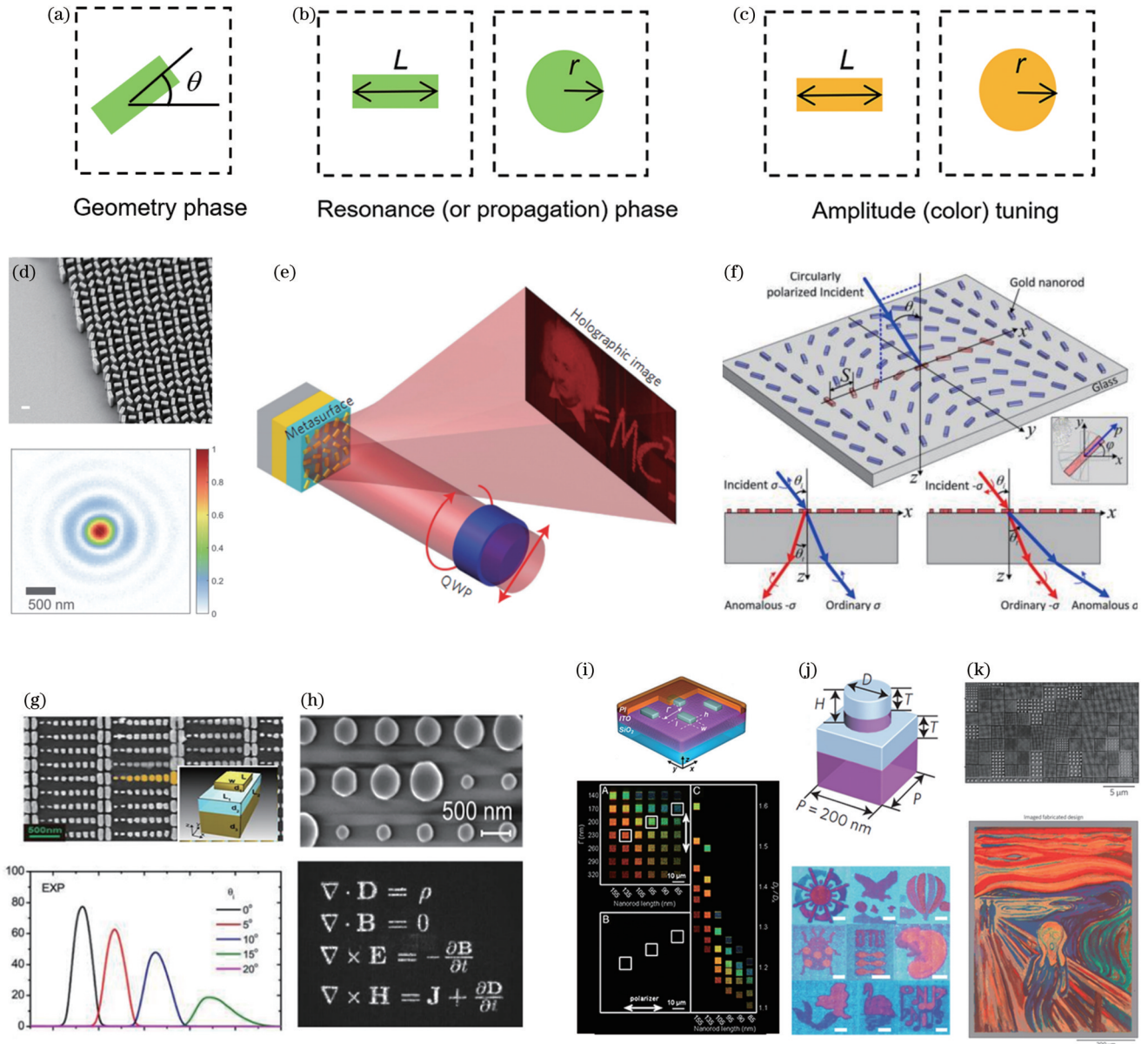


图 2 单自由度琼斯矩阵超构表面结构设计及应用。(a)基于纳米棒转角自由度的几何相位,以及(b)(c)改变结构尺寸,包括改变纳米棒的长短轴或者圆盘的半径,实现共振(或传输)相位调控或者振幅调控,从而实现单自由度琼斯矩阵的单元结构设计;基于几何相位的(d)超透镜功能^[35]、(e)高效率全息^[45]和(f)反常折射现象^[52];基于共振或传输相位的(g)反常反射^[67]和(h)全息^[73]; (i)改变纳米棒长度^[82],以及(j)(k)改变圆盘半径^[84, 90]来实现全彩结构色

Fig. 2 Structure design and applications of Jones matrix metasurface with one degree of freedom. Unit design of Jones matrix with one degree of freedom (a) by geometric phase based on the rotational angle of nanorod, and (b) (c) by changing the structure size, including the length long and short axes of the nanorod or the radius of the disk, to achieve resonance (or propagation) phase or amplitude modulation; optical functionalities of (d) metasurfaces^[35], (e) high efficiency hologram^[45], and (f) anomalous refraction^[52] based on geometric phase; optical functionalities of (g) anomalous reflection^[67] and (h) hologram^[73] based on resonance or propagation phase; full-color printing based on amplitude modulation by (i) changing the length of nanorod^[82] and (j) (k) the radius of disk^[84, 90]

$$E^{\text{out}} = J \begin{bmatrix} 1 \\ \pm i \end{bmatrix} = \cos \frac{\varphi_1 - \varphi_2}{2} \exp[i(\varphi_1 + \varphi_2)/2] \begin{bmatrix} 1 \\ \pm i \end{bmatrix} + i \sin \frac{\varphi_1 - \varphi_2}{2} \exp[i(\varphi_1 + \varphi_2)/2] \exp(\pm i2\theta) \begin{bmatrix} 1 \\ \mp i \end{bmatrix}. \quad (2)$$

可以看到,与入射光偏振态相同的出射光分量所附加的相位与 θ 无关,与入射光偏振态相反的出射光则会

附加一项两倍转角 $\pm 2\theta$ 的相位,这就是几何相位的来源。除了该相位外,还会附加一项 $\exp[i(\varphi_1 + \varphi_2)/2]$ 的相位。由 2.1 节单个自由度的讨论可知,结构长短轴的长度不变,因此该相位是恒定的,此时出射光的左右旋分量附加的相位共轭,无法独立调控。如若考虑长短轴的变化,例如 φ_2 固定、 φ_1 可调[图 3(c)],并考虑

转化效率的最大化, $\varphi_1 - \varphi_2 = \pi$, 此时偏振转化的出射光所附加的相位变为 $\varphi_1 \pm 2\theta$ 。基于此, 通过调节 φ_1 和 θ 可以实现左右旋光相位的独立调控, 打破其相互共

轭的限制。图 3(g) 给出了基于此方法的一个例子^[93], 该例子实现了左右旋光反常折射的独立调控, 其左右旋两个偏振态的出射光方向任意可调。

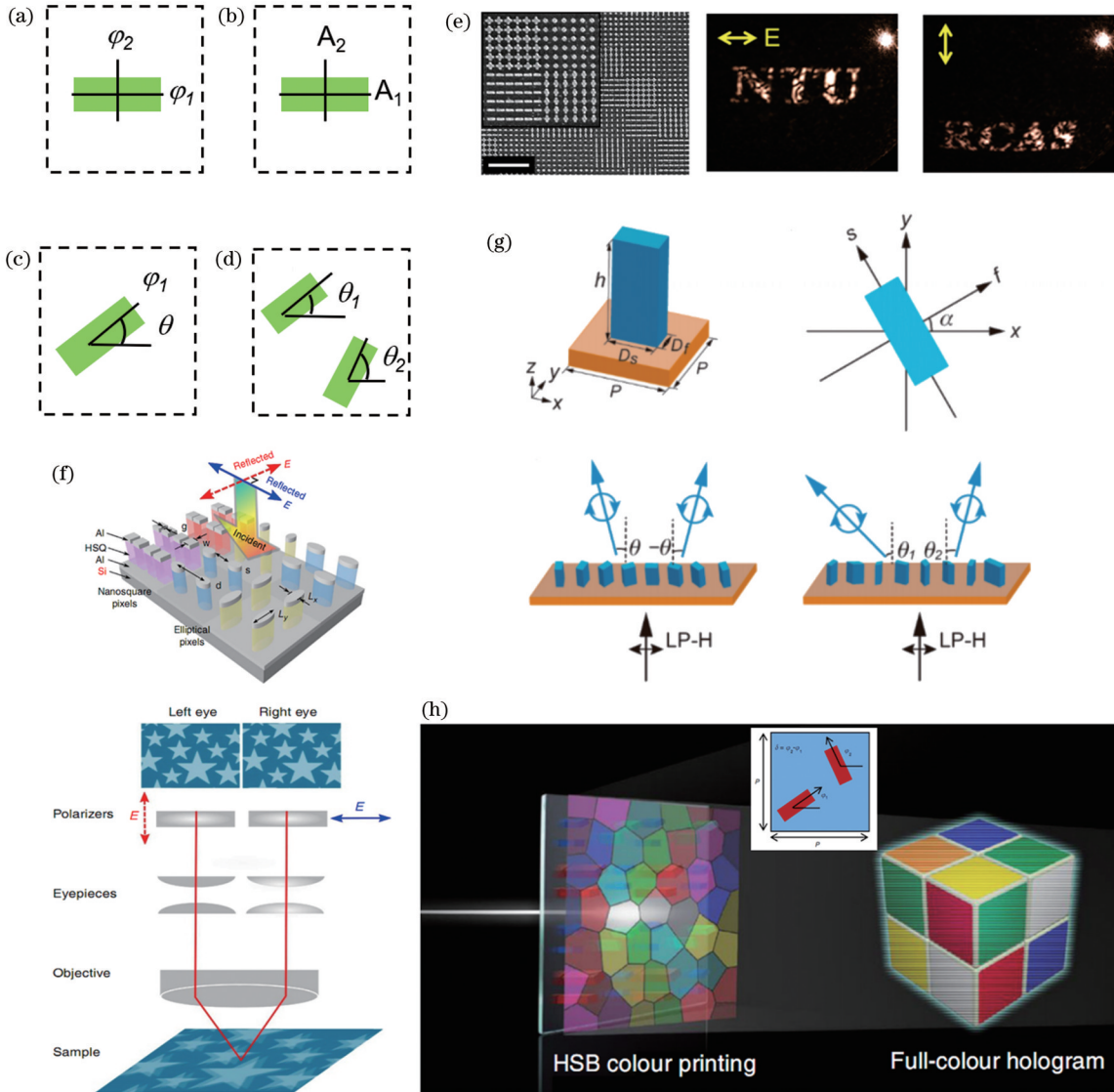


图 3 双自由度琼斯矩阵超构表面结构设计及应用。(a)(b)通过改变纳米棒长短轴长度实现两个正交方向的共振(或传输)相位调控和振幅调控;(c)通过改变纳米棒长轴尺寸和转角自由度实现双自由度琼斯矩阵;(d)基于双纳米棒转角自由度实现琼斯矩阵单个分量的振幅和相位调控;(e)基于图 3(a)的单元结构实现偏振控制的双全息生成^[91];(f)基于图 3(b)的单元结构实现立体 3D 图像显示^[92];(g)基于图 3(c)的单元结构实现左右旋光反常折射角的独立调控^[93];(h)基于图 3(d)的单元结构实现彩色打印图像和全息图像的集成^[32]

Fig. 3 Structure design and applications of Jones matrix metasurface with two degrees of freedom. (a)(b) Realization of resonance (or propagation) phase control and amplitude control in two orthogonal directions based on the size changing of the length of long and short axes of the nanorod; (c) realization of Jones matrix metasurface with two degrees of freedom based on the size change of the length of long axis of the nanorod and the rotational angle; (d) amplitude and phase control of one component of Jones matrix based on the rotation-angle freedom of two nanorods; (e) polarization controlled dual holographic images^[91] based on unit structure in Fig. 3(a); (f) stereoscopic 3D image display^[92] based on the unit structure of Fig. 3(b); (g) independent control of the anomalous refraction angles of the left and right circular polarizations^[93] based on the unit structure in Fig. 3(c); (h) integration of color printing and holographic image^[32] based on the unit structure in Fig. 3(d)

除了单个纳米棒结构,可以在一个单元中考虑多个子结构的共同作用,例如图 3(d)所示的两个纳米棒

结构,并只考虑转角自由度 θ_1 和 θ_2 。在圆偏振光入射下,偏振转化的出射光复振幅为

$$E^{\text{out}} = \exp(\pm i2\theta_1) + \exp(\pm i2\theta_2) = \cos \frac{\theta_1 - \theta_2}{2} \exp[\pm i(\theta_1 + \theta_2)/2]. \quad (3)$$

此时其振幅和相位都可以独立调控,相应的琼斯矩阵有两个自由度,即非对角分量的振幅和相位(圆偏振基矢下)。2019年,本课题组利用该结构,并结合多波长复用技术,实现了彩色的打印图像与全息图像的集成^[32][图 3(h)]。随后,有多项工作^[94-99]报道了类似的不同类型图像的集成功能。基于振幅和相位的双自由度调控,超构表面还应用于提升全息质量^[100-104]、全息加密^[105]、多级衍射调控^[106]等。

2.3 三自由度

在考虑纳米棒所有的几何自由度[图 4(a)]后,即可构造 3 个自由度的琼斯矩阵。纳米棒这一特殊形式的琼斯矩阵[式(1)]能够实现意想不到的光场调控^[107-117]。2015年,Faraon 课题组^[113]证明该酉对称琼斯矩阵可实现任意的偏振和相位转换;2017年,Capasso 课题组^[114]证明了其能够对任意两个正交偏振态施加独立的相位调控,同时转化为相反手性的偏振光,即 $J\lambda^+ = e^{i\varphi_1}(\lambda^+)^*$ 且 $J\lambda^- = e^{i\varphi_2}(\lambda^-)^*$, $\{\lambda^+, \lambda^-\}$ 为相互正交,*表示复共轭,即手性相反。基于此,他们在实验上验证了左右旋入射光下的独立全息[图 4(b)]。当然这一功能可推广到任意的正交偏振态,而不仅仅是正交圆偏振态。如果仅局限于圆偏振态,前面提到的两个自由度即可实现。2020年,Fan 等^[115]将其推广到独立振幅调控。他们在一个单元结构中考虑两个纳米棒,由于每个结构能够对任意正交偏振态施加独立的相位调控,干涉叠加后[类似于式(3)]可实现对任意正交偏振态独立的振幅调控。图 4(c)给出了实现任意正交偏振态的独立振幅调控实验结果,在左右旋入射光下均可观测到独立的打印图像。同年,该团队也基于该琼斯矩阵实现了图像常规成像和边界探测两种模式的自旋切换^[116]。

3 个自由度琼斯矩阵可以用于实现三个分量的独立全息图^[117],如图 4(d)所示。当入射光为 x 偏振,探测光为 x 偏振时,生成“X”全息图;当入射光为 x (或 y)偏振,探测光为 y (或 x)偏振时,生成“Y”全息图;当入射光为 y 偏振,探测光为 y 偏振时,生成“Z”全息图,其对应的琼斯矩阵为 $\begin{bmatrix} e^{i\beta_1} & e^{\beta_2} \\ \sim & e^{i\beta_3} \end{bmatrix}$ 。该琼斯矩阵同样可由单个纳米棒构造,其琼斯矩阵[式(1)]展开式包含 3 个自由度,是关于转角 θ 、传输相位 φ_1 和 φ_2 的复杂表达式,若只考虑相位,可以等价于 $\begin{bmatrix} e^{i\beta_1} & e^{\beta_2} \\ \sim & e^{i\beta_3} \end{bmatrix}$,其中 β_i 与 θ 、 φ_1 、 φ_2 的关系可以通过 3 个方程组进行求解。因此,基于单个纳米棒的结构设计,可以实现不同偏振态组合下的 3 个独立相位调控。

2.4 四自由度

一种典型的具有 4 个自由度的琼斯矩阵表达式为 $\begin{bmatrix} \sim & A_1 e^{i\beta_1} \\ \sim & A_2 e^{i\beta_2} \end{bmatrix}$,当入射光为 y 偏振态时,其出射光为 $[A_1 e^{i\beta_1} \quad A_2 e^{i\beta_2}]^T$,即生成具有任意振幅、相位和偏振态的光场。有趣的是,该琼斯矩阵同样可由单个纳米棒构造[图 5(a)]。一个只有 3 个几何自由度的结构如何实现四自由度琼斯矩阵超构表面构造?首先,将任意光场在左右旋光为基矢的条件下进行展开[图 5(b)],即

$$E = A_1 e^{ix} |R\rangle + A_2 e^{ix} |L\rangle, \quad (4)$$

式中 $|R\rangle$ 和 $|L\rangle$ 表示右旋光和左旋光。对于单个纳米棒,根据式(2),当入射左右旋光时,其出射右旋和左旋光的复振幅分别为 $\sin \frac{\varphi_1 - \varphi_2}{2} \exp[i(\varphi_1 + \varphi_2)/2 + i2\theta]$ 和 $\sin \frac{\varphi_1 - \varphi_2}{2} \exp[i(\varphi_1 + \varphi_2)/2 - i2\theta]$ 。可以看到,两个相位是独立可调的,但振幅相同,无法产生任意的光场。进一步限制 $\varphi_1 + \varphi_2 = 0$,只考虑 φ_1 和 θ 的变化[2 个几何自由度,图 5(a)],此时复振幅为 $\sin \varphi_1 \exp(i2\theta)$ 和 $\sin \varphi_1 \exp(-i2\theta)$,即相互共轭。考虑到这一限制,重新构造右旋光的光场 $(A_1 e^{ix} + A_2 e^{-ix})|R\rangle$,此时左旋光的光场为其共轭场,即 $(A_1 e^{-ix} + A_2 e^{ix})|L\rangle$ [图 5(c)]。由于我们只能想到其中 $A_1 e^{ix}|R\rangle$ 和 $A_2 e^{ix}|L\rangle$ 的分量,故在角谱上需要保证 $A_1 e^{ix}|R\rangle$ 和 $A_2 e^{ix}|L\rangle$ 重合,在空间上可以叠加。同时,需要将 $A_1 e^{ix}|R\rangle$ 和 $A_2 e^{-ix}|R\rangle$ 分开, $A_1 e^{-ix}|L\rangle$ 和 $A_2 e^{ix}|L\rangle$ 分开,因此只需设计 $A_1 e^{ix}$ 和 $A_2 e^{ix}$ 角谱分布范围位于中心点的一侧(可通过附加一个水平波矢),其共轭分布项 $A_1 e^{-ix}$ 和 $A_2 e^{-ix}$ 的角谱将自动移到另一侧,从而实现角谱分离[图 5(c)]。这一角谱偏移的方法同时将零级的非偏振转换分量对测量的影响降到最低。在测量上,入射线偏振光(同时包含左旋和右旋分量),观测一侧光场,即可得到 $A_1 e^{ix}|R\rangle + A_2 e^{ix}|L\rangle$,实现了任意光场生成。由于引入空间角谱,因此利用两个几何自由度的结构就可构造 4 个琼斯矩阵自由度。Zhang 等^[118]基于此实现了具有任意图案和偏振态的矢量光束^[118],如图 5(d)所示。由于在傅里叶空间中观测,共轭光场也会被观测到,且和设计的图案一致。

在单个纳米棒及基础上,实现同样功能的变型结构有很多,如图 5(e)~(h)所示。在单个纳米棒结构实现任意光场的过程中,要求其圆偏振态转换的振幅和相位独立可调。图 5(e)所示为在一个单元中考虑两个相同的纳米棒结构,每个纳米棒具有转角自由度,根据式(3),其具备产生任意光场的条件。基于此可实现多通道、多角度调控的任意空间分布的矢量光场^[119],包括可切换显示的打印图像和全息图像[图 5(i)]。回顾任意光场的表达式——式(4),也可以用两个结构分

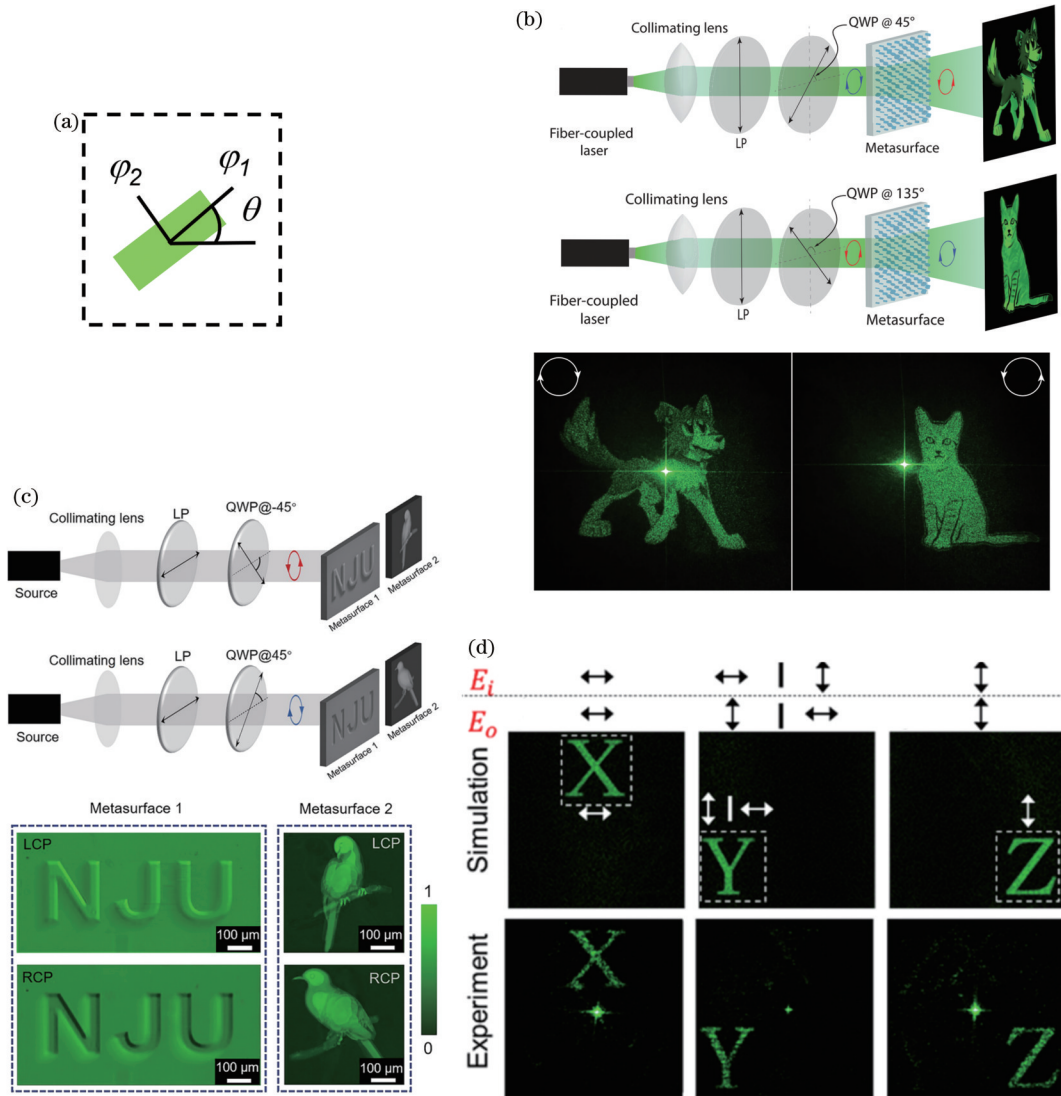


图 4 三自由度琼斯矩阵超构表面结构设计及应用。(a) 基于纳米棒结构长短轴的传输相位和转角自由度实现三自由度琼斯矩阵；(b) 实现任意正交偏振态的独立相位调控^[114]；(c) 实现任意正交偏振态的独立振幅调控^[115]；(d) 基于琼斯矩阵 3 个分量的独立相位调控, 实现在 3 种偏振态组合下的独立全息图像^[117]

Fig. 4 Structure design and applications of Jones matrix metasurface with three degrees of freedom. (a) Realization of three-degree-of-freedom Jones matrix based on two independent transmission phases along the major and minor axes and rotational angle of the nanorod; (b) independent phase control of arbitrary orthogonal polarization states^[114]; (c) independent amplitude control of arbitrary orthogonal polarization state^[115]; (d) independent holographic image under the combination of three incidence-output polarization states based on the independent phase control of three components of Jones matrix^[117]

别实现左旋和右旋偏振态的独立调控, 如图 5(f) 所示。图 5(j) 所示的工作^[120]即采用两个独立的纳米棒结构, 每个结构具有两个自由度, 从而获得任意的矢量光束。进一步地, 将其中的每一个结构替换为两个只有转角自由度的纳米棒, 最终形成由 4 个结构组成的单元[图 5(g)], 同样也可获得任意的矢量光束[图 5(k)]。

除此之外, 还可以采用迂回相位构造类似的琼斯矩阵^[121-124]。如图 5(h) 所示, 一个单元中包含两个结构, 每个结构仅具有转角自由度, 在斜入射光的照射下, 纳米棒的水平坐标位置 x 提供了额外的自由度, 而在出射光场上附加一个迂回相位 $\exp(i2\pi x \sin \gamma / \lambda)$,

其中 γ 为入射角, λ 为波长。2020 年, 本课题组^[121]利用该原理, 在 y 偏振光入射下实现了任意的光场分布, 并应用于完美矢量涡旋光束的生成中[图 5(1)]; 2022 年, 发现该结构能够适用于任意的偏振态入射, 即将任意的偏振态转化任意振幅、相位和偏振态的光场^[122], 从而可应用到偏振转换中。除了上述形式的琼斯矩阵, 具有 4 个自由度的琼斯矩阵还有很多形式, 例如 $\begin{bmatrix} e^{\beta_1} & e^{\beta_2} \\ e^{\beta_3} & e^{\beta_4} \end{bmatrix}$, 由于非对角项不再相同, 无法通过单层结构进行构造, 需要考虑多层结构。可通过构造五层的金属结构^[125], 在微波频段实现了 4 个不同偏振通道下的独立光场操控。

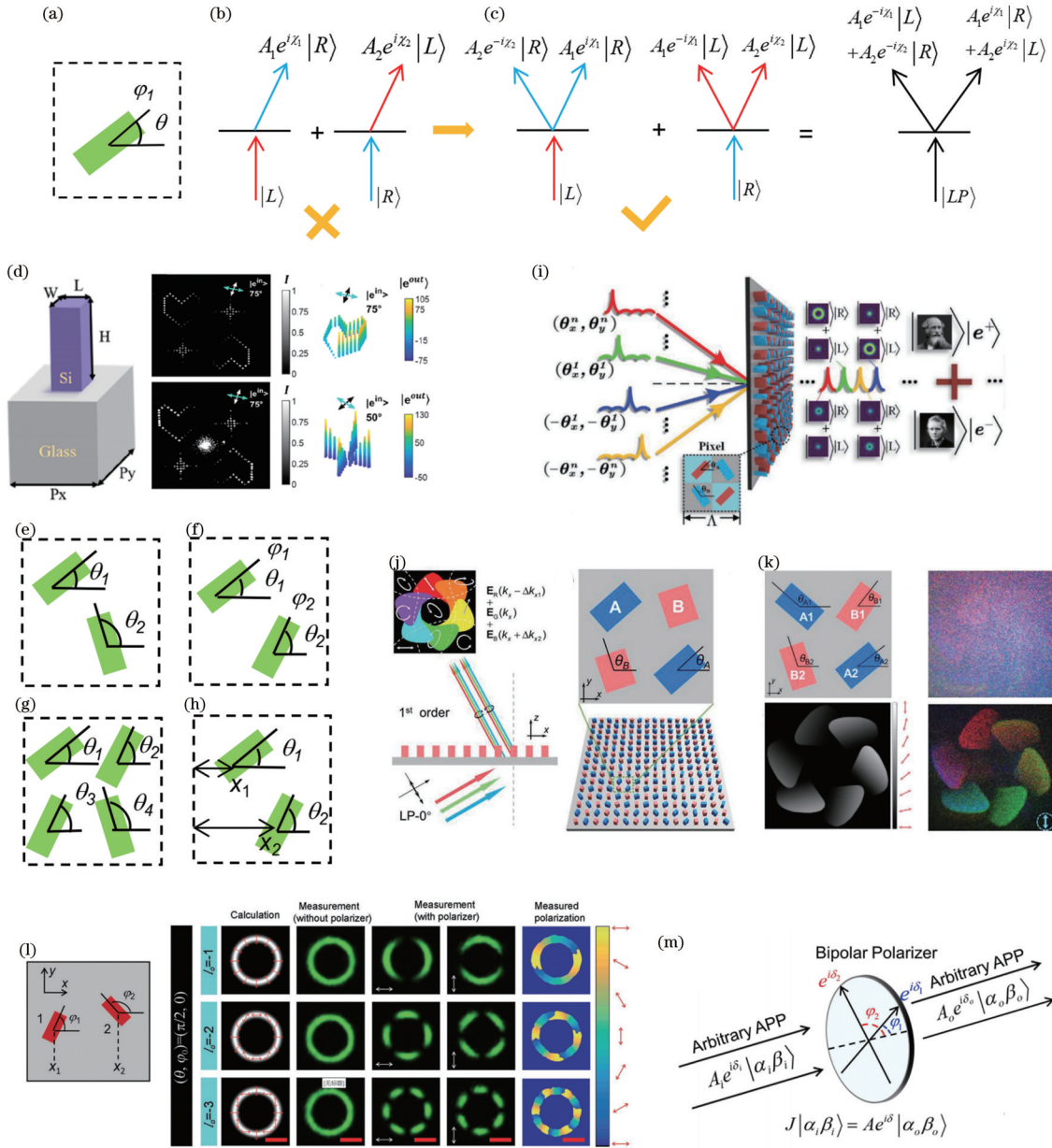


图 5 四自由度琼斯矩阵超构表面结构设计及应用。(a)具有转角自由度和一个方向的传输相位自由度的纳米棒结构示意图；(b)产生任意振幅、相位和偏振态光场示意图,但不满足几何相位约束条件；(c)满足几何相位约束条件产生任意光场示意图；(d)基于单个纳米棒结构产生任意光场,生成具有任意图案和偏振态的矢量光束^[118]；(e)~(h)其他基于图 5(a)纳米棒变型的结构实现任意光场,其中图 5(h)中引入了迂回相位；(i)基于图 5(e)单元结构生成任意光场,实现多通道、多角度调控的任意空间分布的矢量光场^[119]；(j)基于图 5(f)单元结构实现任意光场^[120]；(k)基于图 5(g)单元结构实现任意光场^[120]；(l)基于图 5(h)单元结构实现任意光场,并应用于完美矢量涡旋光束产生^[121]；(m)基于图 5(h)单元结构实现对任意振幅、相位和偏振态之间的转化^[122]

Fig. 5 Structure design and applications of Jones matrix metasurface with four degrees of freedom. (a) Schematic of nanorod with rotational-angle degree of freedom and transmission-phase degree of freedom along one direction; (b) diagram of generating optical field with arbitrary amplitude, phase, and polarization, which does not meet the geometric phase constraints; (c) diagram of generating arbitrary optical field which meets the geometric phase constraints; (d) arbitrary optical field generation to realize vector beam with arbitrary patterns and polarization states^[118] based on single nanorod structure; (e) - (h) other structures based on the nanorod in Fig. 5(a) to realize arbitrary optical field, where the detour phase is introduced in Fig. 5(h); (i) arbitrary optical field generation to realize multi-channel and multi-angle optical control^[119] based on the unit structure in Fig. 5(e); (j) arbitrary optical field generation^[120] based on the unit structure in Fig. 5(f); (k) arbitrary optical field generation^[120] based on the unit structure in Fig. 5(g); (l) arbitrary optical field generation to realize perfect vector vortex beam^[121] based on the unit structure in Fig. 5(h); (m) conversion between two arbitrary amplitude, phase, and polarization states^[122] based on the unit structure in Fig. 5(h)

2.5 六自由度

由于单层结构具有对称性,其琼斯矩阵的非对角项必然相同,它是一个对称矩阵,因此具有最高 6 个自由度,即

$$\begin{bmatrix} A_1 e^{i\beta_1} & A_2 e^{i\beta_2} \\ \sim & A_3 e^{i\beta_3} \end{bmatrix} \text{ 可以证明}^{[126-127]}$$

$$\begin{bmatrix} A_1 e^{i\beta_1} & A_2 e^{i\beta_2} \\ \sim & A_3 e^{i\beta_3} \end{bmatrix} = R(-\theta_1) \begin{bmatrix} e^{i\varphi_1} & 0 \\ 0 & e^{i\varphi_2} \end{bmatrix} R(\theta_1) + R(-\theta_2) \begin{bmatrix} e^{i\varphi_3} & 0 \\ 0 & e^{i\varphi_4} \end{bmatrix} R(\theta_2), \quad (5)$$

等式右边两项即为纳米棒的琼斯矩阵表达式,因此可以在一个单元中放置两个纳米棒结构来实现六自由度的琼斯矩阵构造[图 6(a)].由于每个纳米棒结构有 3 个几何自由度,一个单元共有 6 个几何自由度,满足实现琼斯矩阵所需自由度数量的要求。2021 年, Capasso 课题组^[126]利用该结构实现了在传播方向上任意的连续偏振变化。如图 6(c)所示,实验上测量得到的透射光场在不同距离具有不同的线偏振态的连续变化,同时保持聚焦的强度分布。

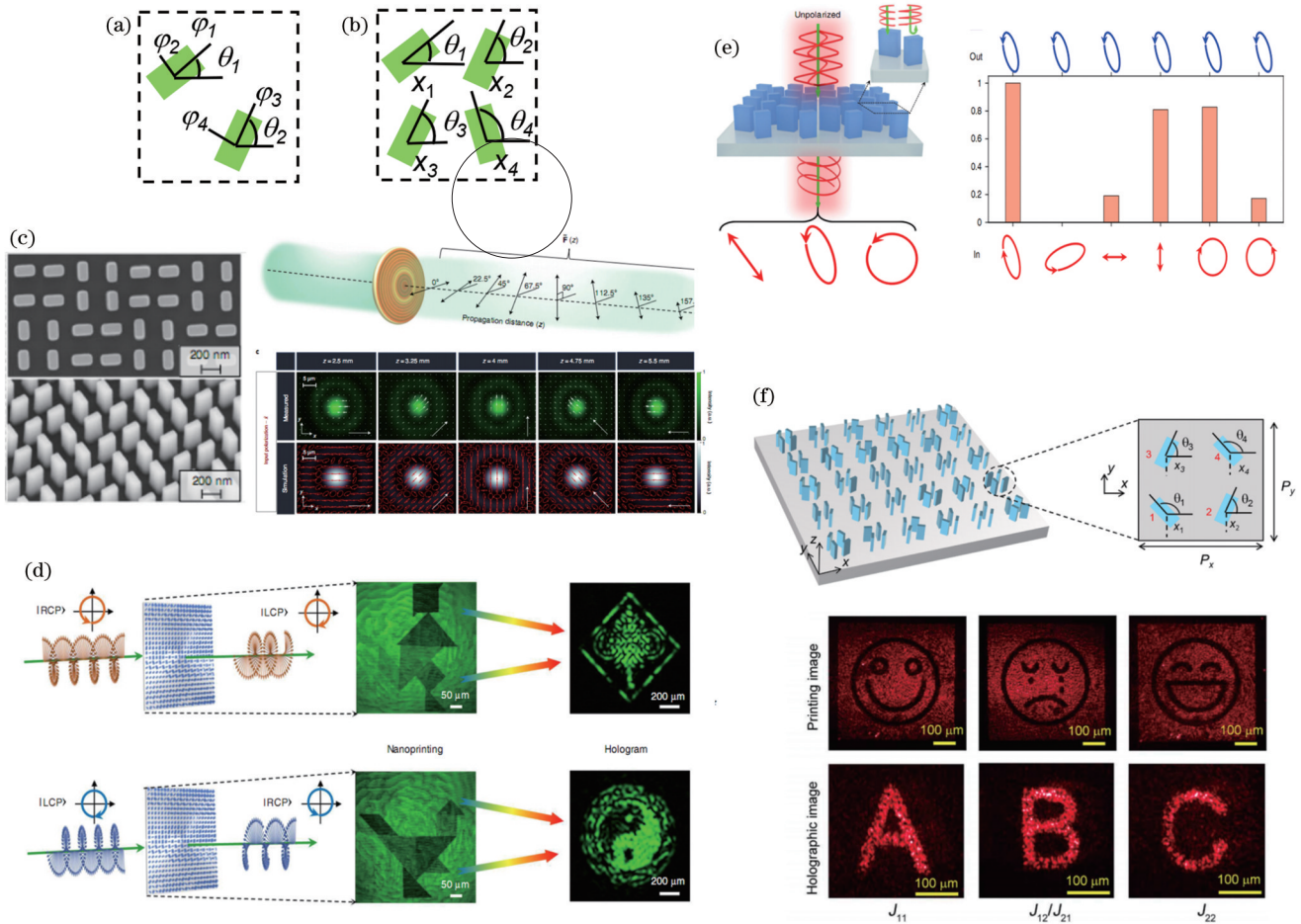


图 6 六自由度琼斯矩阵超构表面结构设计及应用。(a)利用两个纳米棒结构实现六自由度琼斯矩阵的单元结构设计,每个结构具有完整的 3 个自由度,包括转角和长短轴方向的传输相位;(b)利用 4 个纳米棒结构实现六自由度琼斯矩阵的单元结构设计,每个纳米棒只考虑其转角自由度,并引入其位置依赖的迂回相位;(c)基于图 6(a)单元结构实现在传播方向上任意的连续偏振变化^[126];(d)基于图 6(a)单元结构实现任意正交偏振态下独立振幅和相位调控^[128];(e)基于图 6(a)单元结构实现任意偏振态转化为同一种偏振态功能^[129];(f)基于图 6(b)单元结构的六自由度琼斯矩阵,在 3 种不同偏振态的组合下(xx 、 yy 、 xy/yx)实现独立的打印和全息图像集成^[127]

Fig. 6 Structure design and applications of Jones matrix metasurface with six degrees of freedom. (a) Design of unit structure to realize Jones matrix with six degrees of freedom using two nanorod structures, each with three complete degrees of freedom, including two transmission phases along the major and minor axes and the rotation-angle degree of freedom; (b) design of unit structure to realize Jones matrix with six degrees of freedom using four nanorod structures, which only considering its rotation-angle degrees of freedom and position-dependent detour phase; (c) continuous polarization change in the propagation direction^[126] based on the unit structure of Fig. 6(a); (d) independent amplitude and phase control of arbitrary orthogonal polarization state^[128] based on the unit structure in Fig. 6(a); (e) conversion of any polarization state into the same polarization state^[129] based on the unit structure in Fig. 6(a); (f) independent printing and holographic image integration under the combination of three different incidence-output polarization states (xx , yy , and xy/yx)^[127] based on the unit structure in Fig. 6(b)

由于单个纳米棒可以实现对任意正交偏振态的独立相位调控,根据式(3),两个纳米棒的组合可以实现对任意正交偏振态的振幅和相位独立调控,即满足 $J\lambda^+ = A_1 e^{i\varphi_1}(\lambda^+)^*$ 和 $J\lambda^- = A_2 e^{i\varphi_2}(\lambda^-)^*$ 。该表达式的琼斯矩阵为对称矩阵,包含 6 个自由度。Liu 等^[128] 据此实现了在两个正交偏振态下独立的打印图像和全息图像的集成[图 6(d)]。选取 $A_1 = 0, A_2$ 为最大值,由于任意偏振态都可表示为 λ^+ 和 λ^- 的叠加,则光场通过该结构后,其透射光只有一种偏振态 $(\lambda^-)^*$,即可将任意偏振态转化为同一种偏振态[图 6(e)]^[129]。

2021 年,本课题组^[127] 采用迂回相位和转角自由度组合,在一个单元中考虑 4 个纳米棒的结构[图 6(b)],共有 8 个自由度,同样也获得具有 6 个自由度的琼斯矩阵。由于结构几何自由度大于构造的琼斯矩阵自由度,因此对于给定的琼斯矩阵会存在多个解。基于此设计,在 3 种不同偏振态的组合下($xx, yy, xy/yx$),实现了独立的打印和全息图像集成[图 6(f)]。

2.6 八自由度

琼斯矩阵最多具有 8 个自由度,实现这一最高目标具有重要意义。2022 年,本课题组^[130] 和韩国 Shin 课题组^[131] 采用不同方案同时实现了这一目标。由于琼斯矩阵的非对角项相异,必须采用多层结构设计。在

Shin 课题组的方案中,他们首先考虑两个纳米棒结构,分别处于上、下两层[图 7(a)],其琼斯矩阵为 $J_1 \cdot J_2$,其中 J_1 和 J_2 分别为第一层和第二层纳米棒结构的琼斯矩阵。 J_1 和 J_2 都为对称幺正矩阵,其相乘结果为一个任意的幺正矩阵。由于任意 2×2 矩阵可以表示为两个幺正矩阵之和,因此在单元中增加另一组两层纳米棒结构,即可实现任意八自由度的琼斯矩阵。图 7(b) 给出了该结构的一种应用,可以在右旋光入射下产生径向偏振的三维螺旋线,左旋光入射下在不同位置生成不同偏振态的全息图。一般而言,琼斯矩阵复振幅计算的是衍射零级的分量。在该设计中,上下两层距离很小,第一层纳米棒结构的散射光中包含各种散射分量并施加在第二层。因此,将两层的琼斯矩阵写成 $J_1 \cdot J_2$ 会带来一定误差,同时还没有考虑到两层结构之间的耦合,无法实现精确的 8 个自由度调控。相比于相位调控实现全息,要实现精确的振幅调控是十分困难的。

本课题组^[130] 采用两层超构表面结构来构造八自由度琼斯矩阵。两层结构之间相距数百微米[图 7(c)],在这种情况下,两层结构之间几乎没有耦合,因此琼斯矩阵相乘是合适的。考虑每层超构表面具有 6 个自由度,整体结构的琼斯矩阵可写为

$$J_{mn}(x_2, y_2) = \sum_{q=1,2} J_{mq}^2(x_2, y_2) \iint_{x_1, y_1} J_{qn}^1(x_1, y_1) \cdot f(x_2 - x_1, y_2 - y_1, z) dx_1 dy_1, \quad (6)$$

式中: J_{qn}^1 and J_{mq}^2 分别为第一层和第二层琼斯矩阵的 qn 分量和 mq 分量; $f(x_2 - x_1, y_2 - y_1, z) = \frac{1}{2\pi} \frac{\exp(ikr)}{r} \frac{z}{r} \left(\frac{1}{r} - i \frac{2\pi}{\lambda} \right)$ 为瑞利-索末菲脉冲响应。基于梯度优化算法,对于给定的任意 8 个自由度的琼斯矩阵分布,都可以得到每一层结构 6 个自由度琼斯矩阵值,并利用图 6(a) 的结构设计单层结构。图 7(d) 给出了在 4 种入射-探测偏振组合(xx, xy, yx, yy) 下设计的打印图像和全息图像集成的实验测量图,与设计图案符合得较好,验证了该结构对琼斯矩阵 8 个自由度的精确调控。

由于拥有完整的 8 个自由度,该结构能够对任意的两个偏振态进行独立振幅和相位调控,同时转化为任意的两种偏振态,即 $J|\alpha_1\rangle = A_1 e^{i\varphi_1} |\beta_1\rangle$ 和 $J|\alpha_2\rangle = A_2 e^{i\varphi_2} |\beta_2\rangle$, 如图 7(e) 所示,这 4 种偏振 $|\alpha_1\rangle, |\alpha_2\rangle, |\beta_1\rangle$ 和 $|\beta_2\rangle$ 可为任意偏振态。相比于单层六自由度的超构表面,八自由度琼斯矩阵则限制 $\langle \alpha_1 | \alpha_2 \rangle = 0, \langle \beta_1 | \beta_2 \rangle = 0, |\alpha_1\rangle^* = |\beta_1\rangle$ 和 $|\alpha_2\rangle^* = |\beta_2\rangle$ 。

3 总结与展望

超构表面对光场具有灵活的操控能力,已被广泛

应用到各种光学器件中,相关的文献众多。本文从超构表面调控的琼斯矩阵自由度出发,将已有研究中实现的各种不同光学功能的超构表面进行归类并总结其相应的设计方法,为人们了解这一领域提供不同的视角。在超构表面这一领域中,设计是关键环节,主要分为两部分:首先,提出所需功能,例如超透镜聚焦、全息、偏振转换等;然后,寻找一种合适的光学调控原理和方法,例如几何相位、传输相位、迂回相位等。琼斯矩阵自由度这一视角将功能和设计方法统一起来,未来随着这一领域的进一步发展,会有更多的新功能和原理方法出现,但其都可以归纳为不同的琼斯矩阵自由度。本文介绍了不同自由度琼斯矩阵的设计方法,为未来新功能超构表面器件设计提供了重要参考。在这一过程中,首先要确定所需功能对应的琼斯矩阵,以及所需的最低自由度。由于更高自由度琼斯矩阵囊括了低自由度琼斯矩阵,我们固然可以用最高的 8 个自由度设计所需功能,但更高自由度琼斯矩阵会增加结构的复杂度以及降低结构的性能,例如,双层结构的设计会导致制备难度增大、光损耗增大、效率降低,因此针对所需功能,应尽量选择最低自由度琼斯矩阵设计。

从琼斯矩阵自由度这一角度来看,目前已实现了

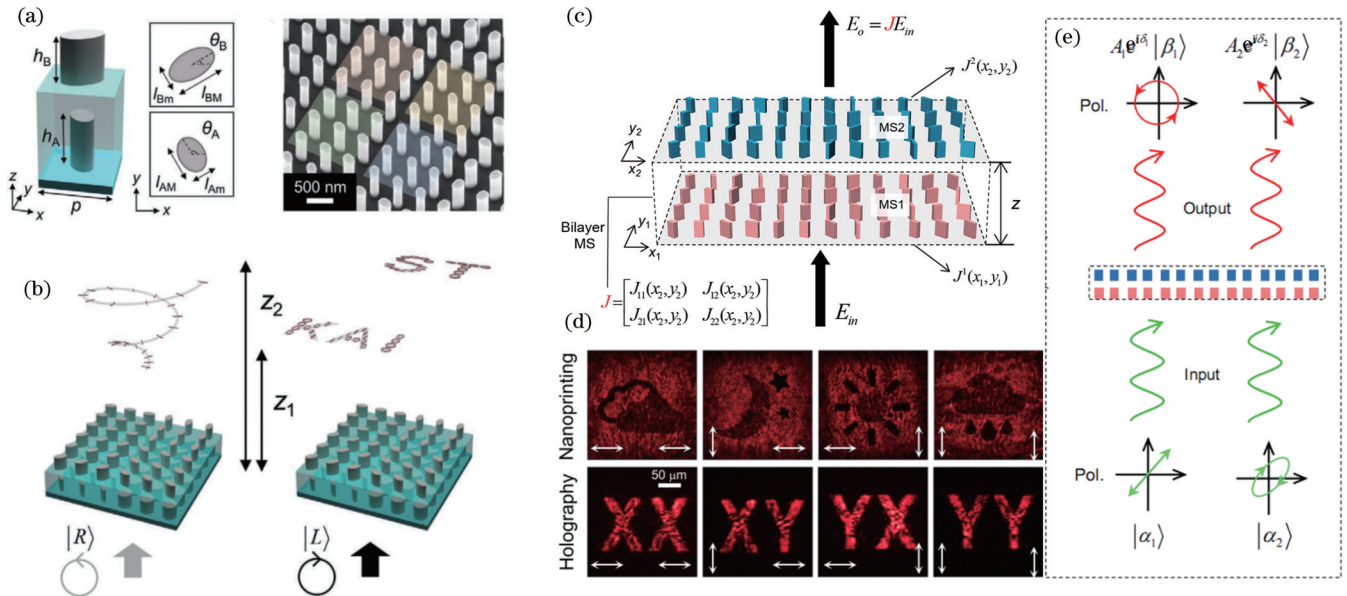


图 7 八自由度琼斯矩阵超构表面结构设计及应用。(a)利用双层紧凑型纳米棒结构实现八自由度琼斯矩阵^[131];(b)基于图 7(a)结构在右旋光入射下产生径向偏振的三维螺旋线,左旋光入射下在不同位置生成不同偏振态的全息图的应用实例^[131];(c)利用双层超构表面结构实现八自由度琼斯矩阵,两层结构相距数百微米^[130];(d)基于图 7(b)结构,在 4 种入射-探测偏振组合 (xx 、 xy 、 yx 、 yy) 下打印图像和全息图像集成的八自由度琼斯矩阵实验测量^[130];(e)基于八自由度琼斯矩阵,实现对任意两个偏振态的独立振幅和相位调控,同时转化为任意两个偏振态的示意图^[130]

Fig. 7 Structure design and applications of Jones matrix metasurface with eight degrees of freedom. (a) Realization of Jones matrix with eight degrees of freedom by double-layer compact nanorod structure^[131]; (b) an application example of producing a 3D spiral pattern with radial polarization under RCP incidence and two different holographic images on different transverse planes with gradually varying polarization states^[131] based on the structure in Fig. 7(a); (c) realization of Jones matrix with eight degrees of freedom by two layer metasurfaces^[130], where the distance between the two layers is hundreds of microns; (d) experimental verification of the Jones matrix with eight degrees of freedom^[130] proposed in Fig. 7(b), where independent printings and holographic images are observed under the four combinations of incident and detection polarization (xx , xy , yx , yy); (e) independent amplitude and phase control on any set of two polarizations and conversions to arbitrary two polarizations^[130] based on the Jones matrix metasurface with eight degrees of freedom

最高 8 个自由度,因此在增加调控自由度的道路上已经走到了尽头,未来可以从如下几个方面进一步研究:

1) 设计新型光学多功能器件。基于已有的多自由度结构的光场操控能力,设计新型光学多功能器件,将多种功能集成到一起,以解决传统设计方法所不能解决的难题。例如,可以将分光、偏振控制、相位调制等不同功能集成融合来构建新型光学器件,这不仅能够提高光场调控的效率和精度,还可以拓展其应用领域,包括光通信、光信息处理、光子学传感等。

2) 高性能多自由度光场操控结构器件。随着光场调控自由度的提升,常常会伴随着性能的降低,例如:为了增大调控自由度,需要增大超构表面的像素尺寸,但会导致衍射角变小;双层结构设计导致损耗增大,效率降低等。因此,设计高性能多自由度的光场操控结构器件是一个重要的研究方向。在结构设计中,需要综合考虑光学器件的能量传输效率、单元结构尺寸、材料特性以及制备工艺等因素,以实现高性能的多自由度光场调控。此外,可以通过计算机辅助优化计算,例如反向拓扑设计^[132-136]等,以满足性能指标为目标,并考虑多种非理想因素的影响,优化设计超构表面器件,

提高光场操控的精度和稳定性。

3) 拓展多自由度琼斯矩阵的波长维度。目前,琼斯矩阵是基于单个波长的光场调控。在实际应用中,多波长的光场调控也具有重要意义,例如实现无色散超透镜^[36, 137]、彩色全息^[43, 76]、颜色分光路由^[138]等。然而,这些多波长调控的自由度都很低,无法实现多个自由度的光场调控。因此,有必要将琼斯矩阵光场调控的多自由度扩展到多波长情况下,实现对波长维度的延伸。这需要考虑结构在不同波长下对光的调控特性变化,包括散射、吸收等,使其满足不同波长下的多自由度调控要求。这些研究将为多波长光场调控提供理论基础和实验方法,推动光场调控技术在多波长应用中的发展,从而在实际中得到更广泛的应用。

参 考 文 献

[1] Yu N F, Genevet P, Kats M A, et al. Light propagation with phase discontinuities: generalized laws of reflection and refraction [J]. Science, 2011, 334(6054): 333-337.
 [2] Sun S L, He Q, Xiao S Y, et al. Gradient-index meta-surfaces as a bridge linking propagating waves and surface waves[J]. Nature Materials, 2012, 11(5): 426-431.
 [3] Zheng P X, Dai Q, Li Z L, et al. Metasurface-based key for

- computational imaging encryption[J]. *Science Advances*, 2021, 7(21): eabg0363.
- [4] Liang C L, Deng L G, Dai Q, et al. Single-celled multifunctional metasurfaces merging structural-color nanoprinting and holography[J]. *Optics Express*, 2021, 29(7): 10737-10748.
- [5] Kim I, Kim W S, Kim K, et al. Holographic metasurface gas sensors for instantaneous visual alarms[J]. *Science Advances*, 2021, 7(15): eabe9943.
- [6] Khaliq H S, Kim I, Kim J, et al. Manifesting simultaneous optical spin conservation and spin isolation in diatomic metasurfaces[J]. *Advanced Optical Materials*, 2021, 9(8): 2002002.
- [7] Engay E, Huo D W, Malureanu R, et al. Polarization-dependent all-dielectric metasurface for single-shot quantitative phase imaging[J]. *Nano Letters*, 2021, 21(9): 3820-3826.
- [8] Cai X D, Tang R, Zhou H Y, et al. Dynamically controlling terahertz wavefronts with cascaded metasurfaces[J]. *Advanced Photonics*, 2021, 3(3): 036003.
- [9] Zhou H Q, Sain B, Wang Y T, et al. Polarization-encrypted orbital angular momentum multiplexed metasurface holography [J]. *ACS Nano*, 2020, 14(5): 5553-5559.
- [10] Yang W H, Xiao S M, Song Q H, et al. All-dielectric metasurface for high-performance structural color[J]. *Nature Communications*, 2020, 11: 1864.
- [11] Su G Y, Liu Y Q. Amplitude-modulated binary acoustic metasurface for perfect anomalous refraction[J]. *Applied Physics Letters*, 2020, 117(22): 221901.
- [12] Shi Z J, Zhu A Y, Li Z Y, et al. Continuous angle-tunable birefringence with freeform metasurfaces for arbitrary polarization conversion[J]. *Science Advances*, 2020, 6(23): eaba3367.
- [13] Li Z L, Chen C, Guan Z Q, et al. Three-channel metasurfaces for simultaneous meta-holography and meta-nanoprinting: a single-cell design approach[J]. *Laser & Photonics Reviews*, 2020, 14(6): 2000032.
- [14] Teng S Y, Zhang Q, Wang H, et al. Conversion between polarization states based on a metasurface[J]. *Photonics Research*, 2019, 7(3): 246-250.
- [15] Song Q H, Baroni A, Sawant R, et al. Ptychography retrieval of fully polarized holograms from geometric-phase metasurfaces [J]. *Nature Communications*, 2020, 11: 2651.
- [16] Ren H R, Briere G, Fang X Y, et al. Metasurface orbital angular momentum holography[J]. *Nature Communications*, 2019, 10: 2986.
- [17] Cordaro A, Kwon H, Sounas D, et al. High-index dielectric metasurfaces performing mathematical operations[J]. *Nano Letters*, 2019, 19(12): 8418-8423.
- [18] Zang X F, Dong F L, Yue F Y, et al. Polarization encoded color image embedded in a dielectric metasurface[J]. *Advanced Materials*, 2018, 30(21): 1707499.
- [19] Yan L B, Zhu W M, Karim M F, et al. Arbitrary and independent polarization control *in situ* via a single metasurface [J]. *Advanced Optical Materials*, 2018, 6(21): 1800728.
- [20] Li J X, Kamin S, Zheng G X, et al. Addressable metasurfaces for dynamic holography and optical information encryption[J]. *Science Advances*, 2018, 4(6): eaar6768.
- [21] Chen H T, Taylor A J, Yu N F. A review of metasurfaces: physics and applications[J]. *Reports on Progress in Physics*, 2016, 79(7): 076401.
- [22] Bukhari S S, Vardaxoglou J, Whittow W. A metasurfaces review: definitions and applications[J]. *Applied Sciences*, 2019, 9(13): 2727.
- [23] Hsiao H H, Chu C H, Tsai D P. Fundamentals and applications of metasurfaces[J]. *Small Methods*, 2017, 1(4): 1600064.
- [24] Yu N F, Capasso F. Flat optics with designer metasurfaces[J]. *Nature Materials*, 2014, 13(2): 139-150.
- [25] Hu J E, Bandyopadhyay S, Liu Y H, et al. A review on metasurface: from principle to smart metadevices[J]. *Frontiers in Physics*, 2021, 8: 586087.
- [26] Ding F, Pors A, Bozhevolnyi S I. Gradient metasurfaces: a review of fundamentals and applications[J]. *Reports on Progress in Physics*, 2018, 81(2): 026401.
- [27] Huang L L, Zhang S A, Zentgraf T. Metasurface holography: from fundamentals to applications[J]. *Nanophotonics*, 2018, 7(6): 1169-1190.
- [28] Song Q H, Liu X S, Qiu C W, et al. Vectorial metasurface holography[J]. *Applied Physics Reviews*, 2022, 9(1): 011311.
- [29] 刘梦蛟, 李添悦, 戈钦, 等. 多功能超构表面的相位调控机制及研究进展[J]. *光学学报*, 2022, 42(21): 2126004.
- Liu M J, Li T Y, Ge Q, et al. Phase modulation mechanism and research progress of multifunctional metasurfaces[J]. *Acta Optica Sinica*, 2022, 42(21): 2126004.
- [30] 华沁怡, 陈心豪, 吕俊鹏, 等. 反射型太赫兹超表面电磁诱导透明效应[J]. *中国激光*, 2021, 48(12): 1214002.
- Hua Q Y, Chen X H, Lü J P, et al. Reflection-type electromagnetically induced transparency effect in terahertz metasurfaces[J]. *Chinese Journal of Lasers*, 2021, 48(12): 1214002.
- [31] Huard S. *Polarization of light*[M]. New York: Wiley, 1997.
- [32] Bao Y J, Yu Y, Xu H F, et al. Full-colour nanoprint-hologram synchronous metasurface with arbitrary hue-saturation-brightness control[J]. *Light: Science & Applications*, 2019, 8: 95.
- [33] Nakamura K. Pancharatnam-Berry phase for polarized light[J]. *Journal of the Physical Society of Japan*, 2013, 82(6): 063701.
- [34] Chen X Z, Chen M, Mehmood M Q, et al. Longitudinal multifoci metalens for circularly polarized light[J]. *Advanced Optical Materials*, 2015, 3(9): 1201-1206.
- [35] Khorasaninejad M, Chen W T, Devlin R, et al. Metalenses at visible wavelengths: diffraction-limited focusing and subwavelength resolution imaging[J]. *Science*, 2016, 352: 1190-1194.
- [36] Wang S M, Wu P C, Su V C, et al. A broadband achromatic metalens in the visible[J]. *Nature Nanotechnology*, 2018, 13(3): 227-232.
- [37] Chen W T, Zhu A Y, Sanjeev V, et al. A broadband achromatic metalens for focusing and imaging in the visible[J]. *Nature Nanotechnology*, 2018, 13(3): 220-226.
- [38] Liang H W, Lin Q L, Xie X S, et al. Ultrahigh numerical aperture metalens at visible wavelengths[J]. *Nano Letters*, 2018, 18(7): 4460-4466.
- [39] Ding X M, Monticone F, Zhang K, et al. Ultrathin Pancharatnam-Berry metasurface with maximal cross-polarization efficiency[J]. *Advanced Materials*, 2015, 27(7): 1195-1200.
- [40] Zhou H P, Chen L, Shen F, et al. Broadband achromatic metalens in the midinfrared range[J]. *Physical Review Applied*, 2019, 11(2): 024066.
- [41] Chen X Z, Huang L L, Mühlenbernd H, et al. Dual-polarity plasmonic metalens for visible light[J]. *Nature Communications*, 2012, 3: 1198.
- [42] Liu H C, Yang B A, Guo Q H, et al. Single-pixel computational ghost imaging with helicity-dependent metasurface hologram[J]. *Science Advances*, 2017, 3(9): e1701477.
- [43] Zhao W Y, Liu B Y, Jiang H, et al. Full-color hologram using spatial multiplexing of dielectric metasurface[J]. *Optics Letters*, 2016, 41(1): 147-150.
- [44] Wen D D, Yue F Y, Li G X, et al. Helicity multiplexed broadband metasurface holograms[J]. *Nature Communications*, 2015, 6: 8241.
- [45] Zheng G X, Mühlenbernd H, Kenney M, et al. Metasurface holograms reaching 80% efficiency[J]. *Nature Nanotechnology*, 2015, 10(4): 308-312.

- [46] Jin L, Dong Z G, Mei S T, et al. Noninterleaved metasurface for (2^6-1) spin- and wavelength-encoded holograms[J]. *Nano Letters*, 2018, 18(12): 8016-8024.
- [47] Wang B, Dong F L, Li Q T, et al. Visible-frequency dielectric metasurfaces for multiwavelength achromatic and highly dispersive holograms[J]. *Nano Letters*, 2016, 16(8): 5235-5240.
- [48] Li X, Chen L W, Li Y, et al. Multicolor 3D meta-holography by broadband plasmonic modulation[J]. *Science Advances*, 2016, 2(11): e1601102.
- [49] Bao Y J, Yan J H, Yang X G, et al. Point-source geometric metasurface holography[J]. *Nano Letters*, 2021, 21(5): 2332-2338.
- [50] Georgi P, Wei Q S, Sain B, et al. Optical secret sharing with cascaded metasurface holography[J]. *Science Advances*, 2021, 7(16): eabf9718.
- [51] Devlin R C, Khorasaninejad M, Chen W T, et al. Broadband high-efficiency dielectric metasurfaces for the visible spectrum[J]. *Proceedings of the National Academy of Sciences of the United States of America*, 2016, 113(38): 10473-10478.
- [52] Huang L L, Chen X Z, Mühlenbernd H, et al. Dispersionless phase discontinuities for controlling light propagation[J]. *Nano Letters*, 2012, 12(11): 5750-5755.
- [53] Liu Z C, Li Z C, Liu Z, et al. High-performance broadband circularly polarized beam deflector by mirror effect of multinanorod metasurfaces[J]. *Advanced Functional Materials*, 2015, 25(34): 5428-5434.
- [54] Jiang S C, Xiong X A, Hu Y S, et al. High-efficiency generation of circularly polarized light via symmetry-induced anomalous reflection[J]. *Physical Review B*, 2015, 91(12): 125421.
- [55] Lin D M, Fan P Y, Hasman E, et al. Dielectric gradient metasurface optical elements[J]. *Science*, 2014, 345(6194): 298-302.
- [56] Zhou J X, Qian H L, Chen C F, et al. Optical edge detection based on high-efficiency dielectric metasurface[J]. *Proceedings of the National Academy of Sciences of the United States of America*, 2019, 116(23): 11137-11140.
- [57] He Q, Zhang F, Pu M B, et al. Monolithic metasurface spatial differentiator enabled by asymmetric photonic spin-orbit interactions[J]. *Nanophotonics*, 2020, 10(1): 741-748.
- [58] Wang R S, He S S, Chen S Z, et al. Computing metasurfaces enabled chiral edge image sensing[J]. *iScience*, 2022, 25(7): 104532.
- [59] Pu M B, Li X, Ma X L, et al. Catenary optics for achromatic generation of perfect optical angular momentum[J]. *Science Advances*, 2015, 1(9): e1500396.
- [60] Maguid E, Yulevich I, Veksler D, et al. Photonic spin-controlled multifunctional shared-aperture antenna array[J]. *Science*, 2016, 352(6290): 1202-1206.
- [61] Zeng J W, Li L, Yang X D, et al. Generating and separating twisted light by gradient-rotation split-ring antenna metasurfaces[J]. *Nano Letters*, 2016, 16(5): 3101-3108.
- [62] Yue F Y, Wen D D, Zhang C M, et al. Multichannel polarization-controllable superpositions of orbital angular momentum states[J]. *Advanced Materials*, 2017, 29(15): 1603838.
- [63] Huang L L, Song X, Reineke B, et al. Volumetric generation of optical vortices with metasurfaces[J]. *ACS Photonics*, 2017, 4(2): 338-346.
- [64] Yin X, Ye Z, Rho J, et al. Photonic spin Hall effect at metasurfaces[J]. *Science*, 2013, 339(6126): 1405-1407.
- [65] Pors A, Albrektsen O, Radko I P, et al. Gap plasmon-based metasurfaces for total control of reflected light[J]. *Scientific Reports*, 2013, 3: 2155.
- [66] Yu N F, Aieta F, Genevet P, et al. A broadband, background-free quarter-wave plate based on plasmonic metasurfaces[J]. *Nano Letters*, 2012, 12(12): 6328-6333.
- [67] Sun S L, Yang K Y, Wang C M, et al. High-efficiency broadband anomalous reflection by gradient meta-surfaces[J]. *Nano Letters*, 2012, 12(12): 6223-6229.
- [68] Pors A, Nielsen M G, Eriksen R L, et al. Broadband focusing flat mirrors based on plasmonic gradient metasurfaces[J]. *Nano Letters*, 2013, 13(2): 829-834.
- [69] Lin J A, Genevet P, Kats M A, et al. Nanostructured holograms for broadband manipulation of vector beams[J]. *Nano Letters*, 2013, 13(9): 4269-4274.
- [70] Li Z Y, Palacios E, Butun S, et al. Visible-frequency metasurfaces for broadband anomalous reflection and high-efficiency spectrum splitting[J]. *Nano Letters*, 2015, 15(3): 1615-1621.
- [71] Aieta F, Genevet P, Yu N F, et al. Out-of-plane reflection and refraction of light by anisotropic optical antenna metasurfaces with phase discontinuities[J]. *Nano Letters*, 2012, 12(3): 1702-1706.
- [72] Aieta F, Genevet P, Kats M A, et al. Aberration-free ultrathin flat lenses and axicons at telecom wavelengths based on plasmonic metasurfaces[J]. *Nano Letters*, 2012, 12(9): 4932-4936.
- [73] Wang L, Kruk S, Tang H Z, et al. Grayscale transparent metasurface holograms[J]. *Optica*, 2016, 3(12): 1504-1505.
- [74] Khorasaninejad M, Ambrosio A, Kanhaiya P, et al. Broadband and chiral binary dielectric meta-holograms[J]. *Science Advances*, 2016, 2(5): e1501258.
- [75] Ni X J, Kildishev A V, Shalaev V M. Metasurface holograms for visible light[J]. *Nature Communications*, 2013, 4: 2807.
- [76] Wan W W, Gao J E, Yang X D. Full-color plasmonic metasurface holograms[J]. *ACS Nano*, 2016, 10(12): 10671-10680.
- [77] Zhang X Q, Tian Z, Yue W S, et al. Broadband terahertz wave deflection based on C-shape complex metamaterials with phase discontinuities[J]. *Advanced Materials*, 2013, 25(33): 4567-4572.
- [78] Zhou Z P, Li J T, Su R B, et al. Efficient silicon metasurfaces for visible light[J]. *ACS Photonics*, 2017, 4(3): 544-551.
- [79] Zhao W Y, Jiang H, Liu B Y, et al. Dielectric Huygens' metasurface for high-efficiency hologram operating in transmission mode[J]. *Scientific Reports*, 2016, 6: 30613.
- [80] Su X F, Li G H, Yang H, et al. A visible high efficiency and polarization-insensitive 34-level dielectric metasurface hologram[J]. *RSC Advances*, 2017, 7(42): 26371-26376.
- [81] Cheng F, Gao J, Luk T S, et al. Structural color printing based on plasmonic metasurfaces of perfect light absorption[J]. *Scientific Reports*, 2015, 5: 11045.
- [82] Olson J, Manjavacas A, Liu L F, et al. Vivid, full-color aluminum plasmonic pixels[J]. *Proceedings of the National Academy of Sciences of the United States of America*, 2014, 111(40): 14348-14353.
- [83] Kumar K, Duan H G, Hegde R S, et al. Printing colour at the optical diffraction limit[J]. *Nature Nanotechnology*, 2012, 7(9): 557-561.
- [84] Zhu X L, Vannahme C, Højlund-Nielsen E, et al. Plasmonic colour laser printing[J]. *Nature Nanotechnology*, 2016, 11(4): 325-329.
- [85] Xue J C, Zhou Z K, Wei Z Q, et al. Scalable, full-colour and controllable chromotropic plasmonic printing[J]. *Nature Communications*, 2015, 6: 8906.
- [86] Duan X Y, Kamin S, Liu N. Dynamic plasmonic colour display[J]. *Nature Communications*, 2017, 8: 14606.
- [87] Tan S J, Zhang L, Zhu D, et al. Plasmonic color palettes for photorealistic printing with aluminum nanostructures[J]. *Nano Letters*, 2014, 14(7): 4023-4029.
- [88] Roberts A S, Pors A, Albrektsen O, et al. Subwavelength plasmonic color printing protected for ambient use[J]. *Nano Letters*, 2014, 14(2): 783-787.

- [89] Miyata M, Hatada H, Takahara J. Full-color subwavelength printing with gap-plasmonic optical antennas[J]. *Nano Letters*, 2016, 16(5): 3166-3172.
- [90] Flauraud V, Reyes M, Paniagua-Dominguez R, et al. Silicon nanostructures for bright field full color prints[J]. *ACS Photonics*, 2017, 4(8): 1913-1919.
- [91] Chen W T, Yang K Y, Wang C M, et al. High-efficiency broadband meta-hologram with polarization-controlled dual images[J]. *Nano Letters*, 2014, 14(1): 225-230.
- [92] Goh X M, Zheng Y H, Tan S J, et al. Three-dimensional plasmonic stereoscopic prints in full colour[J]. *Nature Communications*, 2014, 5: 5361.
- [93] Xu Y H, Li Q A, Zhang X Q, et al. Spin-decoupled multifunctional metasurface for asymmetric polarization generation[J]. *ACS Photonics*, 2019, 6(11): 2933-2941.
- [94] Zhang F, Pu M B, Gao P, et al. Simultaneous full-color printing and holography enabled by centimeter-scale plasmonic metasurfaces[J]. *Advanced Science*, 2020, 7(10): 1903156.
- [95] Yang W H, Qu G Y, Lai F X, et al. Dynamic bifunctional metasurfaces for holography and color display[J]. *Advanced Materials*, 2021, 33(36): 2101258.
- [96] Hu Y Q, Luo X H, Chen Y Q, et al. 3D-integrated metasurfaces for full-colour holography[J]. *Light: Science & Applications*, 2019, 8: 86.
- [97] Wen D D, Cadusch J J, Meng J J, et al. Multifunctional dielectric metasurfaces consisting of color holograms encoded into color printed images[J]. *Advanced Functional Materials*, 2020, 30(3): 1906415.
- [98] Li J X, Chen Y Q, Hu Y Q, et al. Magnesium-based metasurfaces for dual-function switching between dynamic holography and dynamic color display[J]. *ACS Nano*, 2020, 14(7): 7892-7898.
- [99] Wei Q S, Sain B, Wang Y T, et al. Simultaneous spectral and spatial modulation for color printing and holography using all-dielectric metasurfaces[J]. *Nano Letters*, 2019, 19(12): 8964-8971.
- [100] Lee G Y, Yoon G, Lee S Y, et al. Complete amplitude and phase control of light using broadband holographic metasurfaces[J]. *Nanoscale*, 2018, 10(9): 4237-4245.
- [101] Overvig A C, Shrestha S, Malek S C, et al. Dielectric metasurfaces for complete and independent control of the optical amplitude and phase[J]. *Light: Science & Applications*, 2019, 8: 92.
- [102] Jiang Q A, Cao L C, Huang L L, et al. A complex-amplitude hologram using an ultra-thin dielectric metasurface[J]. *Nanoscale*, 2020, 12(47): 24162-24168.
- [103] Jiang Q A, Cao L C, Zhang H, et al. Improve the quality of holographic image with complex-amplitude metasurface[J]. *Optics Express*, 2019, 27(23): 33700-33708.
- [104] Jiang Q A, Hu L Y, Geng G Z, et al. Arbitrary amplitude and phase control in visible by dielectric metasurface[J]. *Optics Express*, 2022, 30(8): 13530-13539.
- [105] Ren H R, Fang X Y, Jang J, et al. Complex-amplitude metasurface-based orbital angular momentum holography in momentum space[J]. *Nature Nanotechnology*, 2020, 15(11): 948-955.
- [106] Liu L X, Zhang X Q, Kenney M, et al. Broadband metasurfaces with simultaneous control of phase and amplitude[J]. *Advanced Materials*, 2014, 26(29): 5031-5036.
- [107] Kim I, Jang J, Kim G, et al. Pixelated bifunctional metasurface-driven dynamic vectorial holographic color prints for photonic security platform[J]. *Nature Communications*, 2021, 12: 3614.
- [108] Guo Y H, Zhang S C, Pu M B, et al. Spin-decoupled metasurface for simultaneous detection of spin and orbital angular momenta via momentum transformation[J]. *Light: Science & Applications*, 2021, 10: 63.
- [109] Rubin N A, D'Aversa G, Chevalier P, et al. Matrix Fourier optics enables a compact full-Stokes polarization camera[J]. *Science*, 2019, 365(6448): eaax1839.
- [110] Devlin R C, Ambrosio A, Rubin N A, et al. Arbitrary spin-to-orbital angular momentum conversion of light[J]. *Science*, 2017, 358(6365): 896-901.
- [111] Zhang K A, Yuan Y Y, Ding X M, et al. High-efficiency metalenses with switchable functionalities in microwave region[J]. *ACS Applied Materials & Interfaces*, 2019, 11(31): 28423-28430.
- [112] Liu M Z, Huo P C, Zhu W Q, et al. Broadband generation of perfect Poincaré beams via dielectric spin-multiplexed metasurface[J]. *Nature Communications*, 2021, 12: 2230.
- [113] Arbabi A, Horie Y, Bagheri M, et al. Dielectric metasurfaces for complete control of phase and polarization with subwavelength spatial resolution and high transmission[J]. *Nature Nanotechnology*, 2015, 10(11): 937-943.
- [114] Balthasar Mueller J, Rubin N A, Devlin R C, et al. Metasurface polarization optics: independent phase control of arbitrary orthogonal states of polarization[J]. *Physical Review Letters*, 2017, 118(11): 113901.
- [115] Fan Q B, Liu M Z, Zhang C, et al. Independent amplitude control of arbitrary orthogonal states of polarization via dielectric metasurfaces[J]. *Physical Review Letters*, 2020, 125(26): 267402.
- [116] Huo P C, Zhang C, Zhu W Q, et al. Photonic spin-multiplexing metasurface for switchable spiral phase contrast imaging[J]. *Nano Letters*, 2020, 20(4): 2791-2798.
- [117] Hu Y Q, Li L, Wang Y J, et al. Trichromatic and tripolarization-channel holography with noninterleaved dielectric metasurface[J]. *Nano Letters*, 2020, 20(2): 994-1002.
- [118] Zhang S F, Huang L L, Li X, et al. Dynamic display of full-Stokes vectorial holography based on metasurfaces[J]. *ACS Photonics*, 2021, 8(6): 1746-1753.
- [119] Wang E L, Niu J B, Liang Y H, et al. Complete control of multichannel, angle-multiplexed, and arbitrary spatially varying polarization fields[J]. *Advanced Optical Materials*, 2020, 8(6): 1901674.
- [120] Guo X Y, Zhong J Z, Li B J, et al. Full-color holographic display and encryption with full-polarization degree of freedom[J]. *Advanced Materials*, 2022, 34(3): 2103192.
- [121] Bao Y J, Ni J C, Qiu C W. A minimalist single-layer metasurface for arbitrary and full control of vector vortex beams[J]. *Advanced Materials*, 2020, 32(6): 1905659.
- [122] Bao Y J, Weng Q, Li B J. Conversion between arbitrary amplitude, phase, and polarization with minimal degrees of freedom of metasurface[J]. *Laser & Photonics Reviews*, 2022, 16(2): 2100280.
- [123] Deng Z L, Deng J H, Zhuang X, et al. Diatomic metasurface for vectorial holography[J]. *Nano Letters*, 2018, 18(5): 2885-2892.
- [124] Deng Z L, Jin M K, Ye X, et al. Full-color complex-amplitude vectorial holograms based on multi-freedom metasurfaces[J]. *Advanced Functional Materials*, 2020, 30(21): 1910610.
- [125] Yuan Y Y, Zhang K A, Ratni B, et al. Independent phase modulation for quadruplex polarization channels enabled by chirality-assisted geometric-phase metasurfaces[J]. *Nature Communications*, 2020, 11: 4186.
- [126] Dorrah A H, Rubin N A, Zaidi A, et al. Metasurface optics for on-demand polarization transformations along the optical path[J]. *Nature Photonics*, 2021, 15(4): 287-296.
- [127] Bao Y J, Wen L, Chen Q, et al. Toward the capacity limit of 2D planar Jones matrix with a single-layer metasurface[J]. *Science Advances*, 2021, 7(25): eabh0365.
- [128] Liu M Z, Zhu W Q, Huo P C, et al. Multifunctional metasurfaces enabled by simultaneous and independent control of phase and amplitude for orthogonal polarization states[J]. *Light: Science & Applications*, 2021, 10: 107.
- [129] Wang S, Deng Z L, Wang Y J, et al. Arbitrary polarization

- conversion dichroism metasurfaces for all-in-one full Poincaré sphere polarizers[J]. *Light: Science & Applications*, 2021, 10: 24.
- [130] Bao Y J, Nan F, Yan J H, et al. Observation of full-parameter Jones matrix in bilayer metasurface[J]. *Nature Communications*, 2022, 13: 7550.
- [131] Chang T, Jung J, Nam S H, et al. Universal metasurfaces for complete linear control of coherent light transmission[J]. *Advanced Materials*, 2022, 34(44): 2204085.
- [132] Deng Y, Ren S M, Fan K B, et al. Neural-adjoint method for the inverse design of all-dielectric metasurfaces[J]. *Optics Express*, 2021, 29(5): 7526-7534.
- [133] Mansouree M, Kwon H, Arbabi E, et al. Multifunctional 2.5D metastructures enabled by adjoint optimization[J]. *Optica*, 2020, 7(1): 77-84.
- [134] Lalau-Keraly C M, Bhargava S, Miller O D, et al. Adjoint shape optimization applied to electromagnetic design[J]. *Optics Express*, 2013, 21(18): 21693-21701.
- [135] Phan T, Sell D, Wang E W, et al. High-efficiency, large-area, topology-optimized metasurfaces[J]. *Light: Science & Applications*, 2019, 8: 48.
- [136] Lin Z, Groeuer B, Capasso F, et al. Topology-optimized multilayered metaoptics[J]. *Physical Review Applied*, 2018, 9(4): 044030.
- [137] Lin R J, Su V C, Wang S M, et al. Achromatic metalens array for full-colour light-field imaging[J]. *Nature Nanotechnology*, 2019, 14(3): 227-231.
- [138] Chen B H, Wu P C, Su V C, et al. GaN metalens for pixel-level full-color routing at visible light[J]. *Nano Letters*, 2017, 17(10): 6345-6352.

Design and Application of Jones Matrix Metasurface with Different Degrees of Freedom

Bao Yanjun*, Li Baojun**

Guangdong Provincial Key Laboratory of Nanophotonic Manipulation, Institute of Nanophotonics, Jinan University, Guangzhou 511443, Guangdong, China

Abstract

Significance As a layer of artificially designed two-dimensional planar structure, the metasurface provides a new platform for the miniaturization and integration of optical devices. In recent years, with the continuous development of this field, a variety of optical mechanisms and optical functional devices based on metasurfaces have been proposed. Despite their seemingly diverse functionalities, they can be all attributed to the control of different degrees of freedom in the Jones matrix. The Jones matrix is commonly employed to describe the ability of optical devices to control polarization, amplitude, and phase of light, with a maximum number of eight degrees of freedom. Especially, more controlled degrees of freedom lead to diverse functionalities that can be achieved. For example, a single degree of freedom in the Jones matrix can be adopted for anomalous transmission. By increasing to two degrees of freedom, such as independent control of amplitude and phase of a specific component of the Jones matrix, the integration of color printing and holography can be realized. From the perspectives of the degrees of freedom in the Jones matrix, we classify and summarize the designs and applications of metasurface research in recent years to help researchers better understand the physical mechanisms of different functionalities of metasurfaces.

Progress Our study focuses on the designs and applications of metasurfaces from the perspectives of the degrees of freedom in the Jones matrix. We firstly argue that all the functionalities of metasurfaces can be categorized into different degrees of freedom in Jones matrix and the more controlled degrees of freedom lead to diverse functionalities that can be realized (Fig. 1). Each component of the Jones matrix has two terms of amplitude and phase. Therefore, different mechanisms to control the phases including the geometry phase, resonance phase, and propagation phase are introduced to realize one degree of freedom (Fig. 2), which can be utilized for functionalities of metalens, hologram, and anomalous transmission. By changing the size of nanorods or nanodisks, the amplitude can also be controlled. Next, we show how to employ a simple structure of nanorod to construct multiple degrees of freedom in Jones matrix, including two (Fig. 3), three (Fig. 4), four (Fig. 5), six (Fig. 6), and eight (Fig. 7). Meanwhile, the possible applications are provided.

Conclusions and Prospects We categorize and summarize the design methods of metasurfaces with different optical functionalities based on their degrees of freedom in the Jones matrix to provide different perspectives for the metasurface field. Although the highest number of degrees of freedom of eight in the Jones matrix has been realized, the following points can be explored. First, new optical multifunctional devices should be designed by integrating various functionalities based on the multi-degrees of freedom metasurfaces. Second, the optical performance of metasurface devices with multiple degrees of freedom should be improved. Third, the Jones matrix should be extended to the wavelength dimension to enable multi-wavelength and multi-degrees of freedom control of light fields. With continuous research and deepening exploration, the field of metasurfaces will advance with a wider range of practical applications.

Key words metasurfaces; Jones matrix; multiple degrees of freedom; phase modulation; amplitude modulation